Journal of Nuclear Materials 404 (2010) 121–127

Contents lists available at ScienceDirect

Journal of Nuclear Materials

journal homepage: www.elsevier.com/locate/jnucmat

Effect of impurity and alloying elements on Zr grain boundary strength from first-principles computations

M. Christensen [a], T.M. Angeliu [b], J.D. Ballard [b,*], J. Vollmer [b], R. Najafabadi [b], E. Wimmer [a]

[a] Materials Design, Inc., P.O. Box 1318, Angel Fire, NM 87710-1318, United States
[b] Knolls Atomic Power Laboratory, P.O. Box 1072, Schenectady, NY 12301-1072, United States

ARTICLE INFO

Article history:
Received 30 April 2009
Accepted 2 July 2010

ABSTRACT

Effects of twenty impurity and alloy elements on the strength of a Zr(0 0 0 1)/Zr(0 0 0 1) $\sum$7 twist grain boundary were studied using a first-principles density functional approach. A ranking in the order of most weakening to most strengthening was: Cs, I, He, Te, Sb, Li, O, Sn, Cd, H, Si, C, N, B, U, Ni, Hf, Nb, Cr, and Fe. Segregation energies for these elements to the grain boundary and the Zr(0 0 0 1) surface were also calculated. Calculations showed that the weakening grain boundary elements He, I, and Cs have a strong driving force for segregation to the grain boundary from bulk Zr. Zircaloy cladding failures (pellet-clad interactions) in commercial fuel systems and separate effects test results provide context for these computational results.

1. Introduction

A combination of mechanical properties, corrosion resistance and low neutron absorption cross section makes zirconium-based alloys very important structural materials in the nuclear industry. To maintain functionality of zirconium alloys in nuclear environments, it is important to understand the effects of alloying elements, impurities, and elements resulting from fission, transmutation, and coolant interactions on properties of these alloys. Of particular concern is weakening caused by accumulation of impurities at zirconium grain boundaries. It is known that impurities at parts per million level concentrations in the bulk material could result in a significant reduction of material strength and transition of fracture mode from ductile to brittle.

Resistance of zirconium-based alloys to radiation embrittlement is highly valued in reactor design. Even after significant irradiation, Zircaloy fracture surfaces exhibit ductile fracture features. However, during power transients in commercial nuclear power plants, brittle fracture can occur and is known as pellet-clad interaction (PCI) [1]. The responsible mechanism is believed to be fission product induced stress corrosion cracking, with iodine suspected as the primary detrimental specie. However, mechanistic details for how iodine promotes brittle failure are unknown, with two main mechanisms being proposed [2]. In the first, iodine adsorbed on a crack face lowers the Zr–Zr bond energy leading to separation along crystallographic planes (transgranular cleavage crack path) or grain boundaries (intergranular crack path). In the second mechanism, crack advance occurs by formation of ZrI_4(g) that transports Zr away from the crack tip [3]. The importance of iodine concentration and ZrI_4 partial pressure on SCC (stress corrosion cracking) susceptibility of Zircaloy has been shown in several studies [2,4,5].

Since it is difficult to obtain experimental information on the effects of impurity atoms on grain boundary strength, theory provides useful insight via first-principles calculations. The relative high accuracy of first-principles calculations makes this approach well suited to studying effects of iodine and other elements on the theoretical grain boundary strength. This method has successfully been used to study effects of solutes on interfacial strength in a number of different systems, including potentially detrimental elements P and B in a Fe tilt grain boundary [6], H, B, and P in a Ni tilt grain boundary [7], 16 impurity elements in a Ni $\sum$5(0 0 1) twist grain boundary [8], S in Ni/Al_2O_3 interface [9], and 3*d*-transition metals in WC grain boundaries [10,11].

The present study investigates grain boundary strength of zirconium by twenty different elements. The primary objective is to assess the effects of various elements on the cohesion of a Zr grain boundary to provide insight to mechanisms that may contribute to PCI failures. The following impurities (tramp elements, alloy additions, fission or transmutation products, *etc.*) were studied: H, He, Li, B, C, N, O, Si, Cr, Fe, Ni, Nb, Cd, Sn, Sb, Te, I, Cs, Hf, and U at a concentration of 1 impurity atom per bulk, surface, or grain boundary model. This set of models utilized bounds a range of conditions from behavior in bulk, a low energy grain boundary, and to higher energy boundaries, with a surface being a representation, for screening major trends in Zr and impurity behaviors for the large set of elements analyzed.

* Corresponding author. Tel.: +1 518 395 7865; fax: +1 518 395 4422.
E-mail address: Jake.Ballard@unnpp.gov (J.D. Ballard).

0022-3115/$ - see front matter © 2010 Published by Elsevier B.V.
doi:10.1016/j.jnucmat.2010.07.012

2. Computational method

Computational modeling based on *ab initio* density functional theory (DFT) was used for all calculations [12]. Electron–electron exchange and correlation effects were modeled by the generalized gradient approximation (GGA) with a functional form proposed by Perdew–Burke–Emzerhof (PBE) [13]. Density functional of Kohn–Sham equations were solved with projector-augmented-wave (PAW) potentials [14] as implemented in the Vienna *ab initio* Simulation Package (VASP) version 4.6 [15–18] and integrated in the MedeA computational environment [19]. The plane-wave cutoff energy, which represents the number of plane waves included in calculations, was set to 330 eV. Integration over the Brillouin zone, that represents the number of points included in calculations for each electronic energy bands, was sampled using a Monkhorst–Pack grid with a density of 5 nm^{-1}. The Methfessel–Paxton scheme was used to set partial occupancies with a smearing of 0.2 eV to avoid numerical instability due to partially filled electronic bands in nickel. Equilibrium structures were determined by optimization using a conjugate gradient minimization technique. All geometry optimizations involved the relaxation of all atoms in the system. Convergence tests were performed to ensure that calculated energies converged to within about 1 meV/atom and residual forces were less than (0.1 eV/nm), which is a reasonable balance between computational time and needed accuracy.

2.1. Bulk zirconium model

Computations were first performed on low temperature α-phase (hexagonal close packed, HCP) pure zirconium. Calculations on α-phase were used to assess computational accuracy, and optimized lattice parameters were subsequently used to construct models of zirconium free surfaces and grain boundaries. Starting from the experimental structure [20], lattice parameters of pure α-Zr were computed assuming a hexagonal crystal structure with symmetry $P6_3/mmc$. Bulk Zr lattice parameters were optimized with tighter computational parameters than those used for surface and grain boundary geometry relaxations, where only the atomic positions were optimized and not the cell parameters. This is due to cell optimization relying on a stress tensor, which requires more stringent computational parameters than computation of forces used for the relaxation of atoms in a cell of fixed size. For cell optimization, the *k*-space integration was performed using the tetrahedron method with Blöchl corrections [21] and a *k*-point mesh with density 1 nm^{-1}.

Resulting, optimized, lattice parameters were $a = 0.3233$ nm and $c = 0.5178$ nm. This compares well with experimental results of $a = 0.3231$ nm and $c = 0.5148$ nm [20]. Slightly larger computed lattice parameters compared to experiments are typical for DFT–GGA. Differences between computed and experimental lattice parameters would be slightly larger if the experimental lattice parameters were extrapolated to $T = 0$ K.

2.2. Zirconium grain boundary and surface model

Grain boundary models used in atomistic calculations are generally subjected to periodic boundary conditions in all three directions or at least within the grain boundary plane to avoid surface effects and to reduce the model size (number of atoms). This condition limits grain boundary models to a special class of boundaries called CSL (Coincidence Site Lattice), which are well representative of general boundaries. Unlike for materials with cubic symmetry, the CSL grain boundaries for materials with hexagonal symmetry can only be constructed with their normal along the [0 0 0 1] crystallographic direction. This is due to a lack of translational symmetries in other grain boundaries since the *c*/*a* lattice parameters ratio is in general an irrational number. This study constructed a Zr $\sum 7$ (0 0 0 1) twist grain boundary to reduce computational resources needed while being relatively well representative of general grain boundaries. This model was constructed by cleaving a single crystal along the (0 0 0 1) plane, rotating the top part along the [0 0 0 1] axis by ~36° and then putting the two parts (grains) back together. The constructed twist grain model has its edges along the [1 0 1 0], [1 1 2 0], and [0 0 0 1] crystallographic directions. The grain boundary model has six atomic (0 0 0 2) layers of Zr in each grain, a surface area of about 0.64 nm^2, and a total of 84 atoms. The optimized structure is shown in Fig. 1.

The (0 0 0 1) surface model was constructed by replacing the top grain in the grain boundary model by a vacuum. The surface model, therefore, has the same dimensions as the grain boundary model, but it contains 42 atoms.

2.3. Grain boundary and surface energy calculations

Effect of impurities on Zr ideal grain boundary strength was determined by calculating the total energy of the grain boundary model and the surface model. Various impurity positions (substitutional vs. interstitial) in both the grain boundary and surface models were considered to find their corresponding lowest total energy configurations. The following equation is used to calculate an ideal grain boundary strength (W^x_{Sep}) for impurity element *x*:

$$W^x_{Sep} = (E^x_{s1} + E_{s2} - E^x_{gb})/2A \quad (1)$$

where E^x_{s1} and E_{s2} are total energies for surface models corresponding to two grains, E^x_{gb} is the total energy of a grain boundary model, *A* is a grain surface area, and the factor 2 accounts for presence of two grain boundaries in the model.

The total energy of a pure Zr model containing an impurity element in a substitutional or interstitial site, and the above total grain boundary and surface energies were used to calculate the surface and grain boundary segregation energies using the following equations:

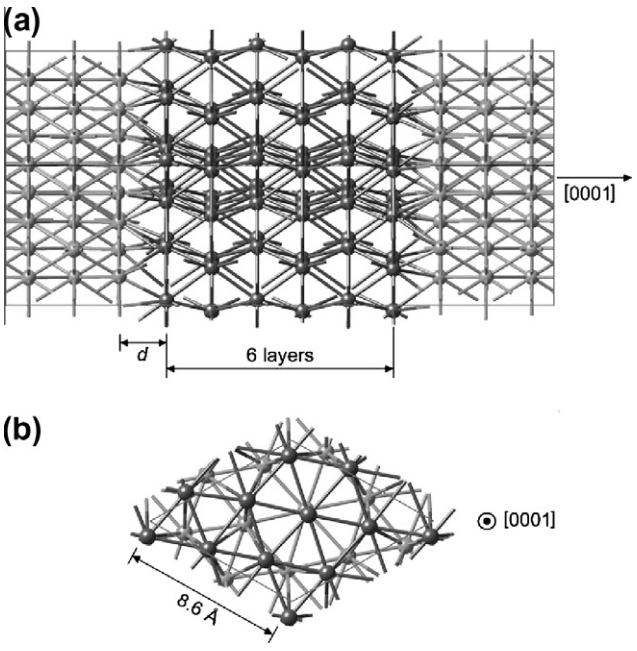

Fig. 1. (a) Side view and (b) top view of the computational model structure of the Zr(0 0 0 1)/Zr(0 0 0 1) $\sum 7$ twist grain boundary. There are seven atoms per atomic layer. Different colors are used for Zr atoms in different grains. The relative positions of two atomic layers in each grain closest to the interface are shown in (b).

$$E^{s}_{seg} = E^{x}_{s} - E^{x}_{p} - E_{s} + E_{p} \quad (2)$$

$$E^{gb}_{seg} = E^{x}_{gb} - E^{x}_{p} - E_{gb} + E_{p} \quad (3)$$

where E_p is the total energy of a pure bulk Zr model, E^x_p is the energy of a bulk model including impurity x, E_{gb} and E_s are the pure grain boundary and surface model energies, respectively, and E^x_{gb}, E^x_s are the grain boundary and surface model energies, respectively, containing impurity x.

3. Computational results

In calculations described here, it is assumed that impurities are present at grain boundaries and stay on surfaces when a boundary is separated into two surfaces. In order to determine the thermodynamic driving force for impurities to segregate from inside the grain to the grain boundary and to the surface, additional calculations were performed. The Zr $\sum$7 (0 0 0 1) twist grain boundary structure as depicted in Fig. 1 has a computed equilibrium distance of d = 0.273 nm between the two Zr grains with very little corrugation of the atomic layers adjacent to the grain boundary as illustrated in Fig. 1. In bulk Zr, the computed distance between the (0 0 0 2) atomic planes is 0.259 nm. The interlayer distances d12, d23, and d34 in the grain boundary are 0.256 nm, 0.264 nm, and 0.258 nm, respectively, with a numerical precision of ±0.002 nm. These atomic spacing values suggest that the strain field associated with this special grain boundary is limited to the few (0 0 0 2) atomic planes adjacent to the grain boundary plane. The calculated grain boundary energy was 0.29 J/m^2. Further calculations using the same grain boundary model but displacing grain A relative to grain B showed that there are many other stable grain boundary configuration with almost identical energies. However, calculations reported here are based on the grain boundary model with no initial relative grain displacement. The calculated work of separation is 2.86 J/m^2 and is identical to that computed by Kwon et al. [22]. Optimized grain boundary shows rather small atomic relaxation in the Zr $\sum$7 grain boundary region, therefore, it is not surprising that this is a rather strong boundary. For comparison, the work of separation for cleavage of bulk Zr along the (0 0 0 1) plane is calculated to be 3.15 J/m^2(twice the value of the Zr(0 0 0 1) surface energy, namely 1.57 J/m^2). The clean grain boundary was the reference when assessing the effect of impurity atoms on grain boundary strength.

3.1. Impurities in bulk zirconium

Before investigating the effects of impurity elements on the grain boundary and its corresponding free surfaces, the energetics and site preference of impurities in bulk zirconium were determined. Preferred sites of impurities in bulk zirconium together with associated heats of formation were computed using low temperature stable phases for impurity elements as reference states. Preferred impurity configurations will be used to determine the segregation energy to the grain boundary and surface. Bulk model calculations with impurities at different sites show that: (i) smaller elements H, B, C, N, and O clearly prefer interstitial sites (ii) He, Si, Cr, Fe, and Ni have no strong site preference between substitutional and interstitial sites, and (iii) Li, Nb, Sn, Cd, Sb, Te, I, Cs, Hf, and U substitute for bulk Zr atoms.

The heat of solution for elemental defects in bulk α-Zr is summarized in Fig. 2, where H, B, C, N, O, Si, Sn, Sb, and Te have a negative heat of formation. A negative value means that it is energetically favorable for these impurities to dissolve in the Zr lattice, either in an interstitial or a substitutional site, if no competing compound phases could form. With increasing temperature, the gain in configurational entropy in the dissolved state generally tends to increase impurity solubility. Computed heats of formation of impurities in α-Zr are consistent with available experimental binary phase diagrams [23]. No phase diagram is reported for I–Zr, Te–Zr or He–Zr in the literature reviewed. In fact, helium is the least stable impurity in Zr in the current set, and together with Cs, these elements have a strong thermodynamic driving force to escape from metallic Zr. The Cs–Zr and Li–Zr phase diagram show that neither Cs nor Li are soluble in Zr.

3.2. Impurities at zirconium (0 0 0 1) surface

Segregation energies were calculated to understand the propensity for impurity atoms to diffuse from their preferred positions in bulk α-Zr to either a free surface or grain boundary. Calculations showed that fifteen of twenty elements studied have a tendency to segregate to the Zr(0 0 0 1) surface while five elements, namely B, C, N, Nb, and Hf have a tendency to remain in the bulk as shown in Fig. 3. Boron, carbon, and nitrogen all occupy octahedral sites in bulk zirconium. At the zirconium surface, these atoms also occupy octahedral interstitial sites, just below the top zirconium atomic layer. However, they form more nearest neighbor bonds in the bulk sites than at the surface and therefore, are somewhat more stable in the bulk resulting in no driving force for surface segregation. It

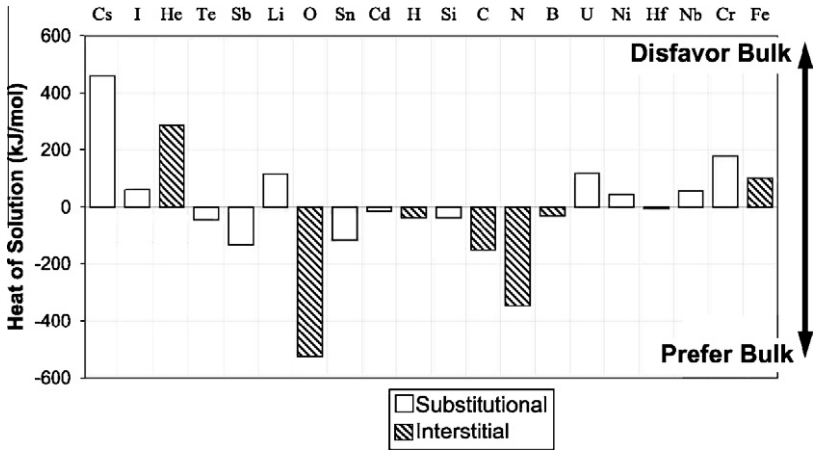

Fig. 2. Heat of solution for elements in α-Zr. A negative value indicates that it is energetically favorable for the impurity to go into solution. The heat of formation is in reference to pure elements in their thermodynamic ground state. Only electronic energies are taken into account.

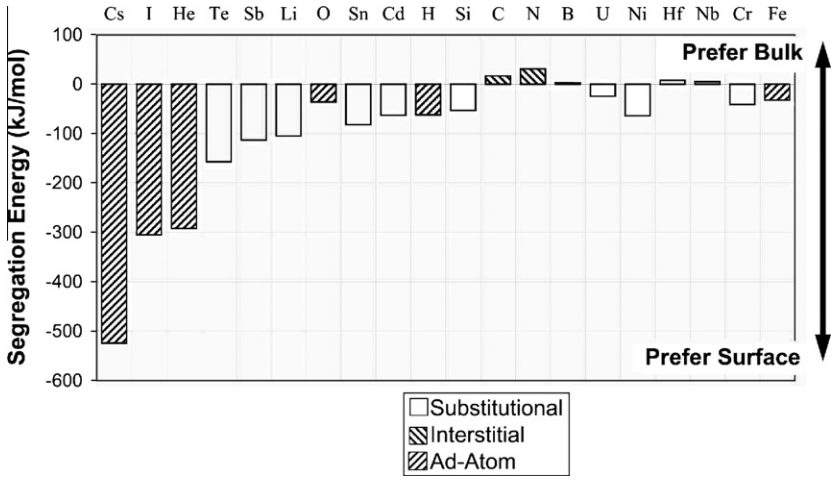

Fig. 3. Summary of element surface segregation energies in α-Zr. Cs, I, He, Te, Sb, and Li have substantial driving forces for surface segregation. C, N, B, Hf, and Nb prefer to remain in the bulk.

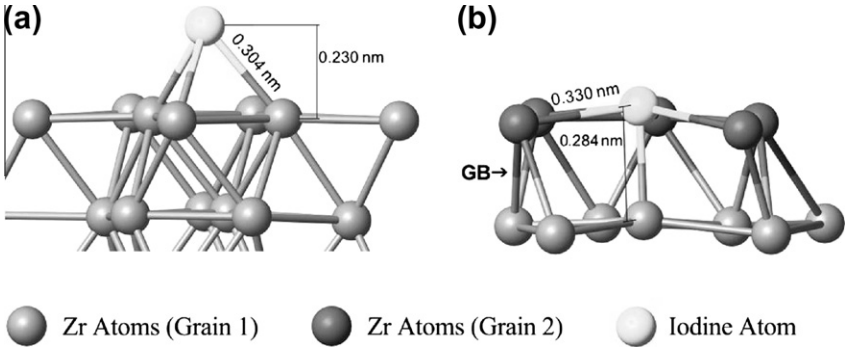

Fig. 4. Preferred locations of iodine: (a) ad-atoms at a Zr free surface (no grain boundary), and (b) substitutional at a Zr grain boundary (GB).

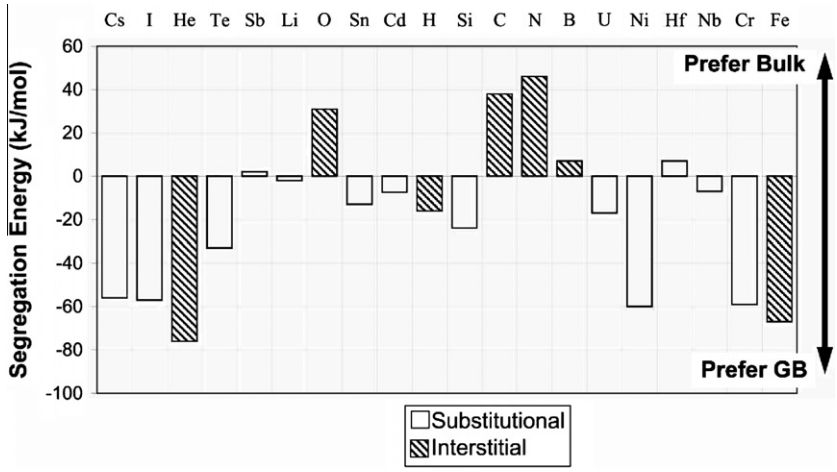

Fig. 5. Summary of grain boundary segregation energies and stable occupancy sites in α-Zr. Cs, I, He, Te, Si, Ni, Cr, and Fe each have a substantial driving force for grain boundary segregation.

should be noted that these results are obtained for the Zr(0 0 0 1) surface and may not hold for other surfaces.

For all other elements studied, there is a driving force for surface segregation, *i.e.*, the system lowers its electronic energy by moving an atom from the bulk to the surface. The element with the largest segregation energy is Cs, with I, He, Te and Sb having significant segregation energies. The most stable site for H, Li, O, Fe, I, and Cs are ad-atom sites on the Zr(0 0 0 1) surface, occupying threefold hollow sites. The preferred ad-atom site for iodine is shown in Fig. 4a. Si, Cr, Ni, Nb, Cd, Sn, Sb, Te, Hf and U are most stable in substitutional sites at the free surface. It should be noted that the present analysis was based strictly on energy considerations and does not include entropic contributions that may be important at high temperature. However, it is not expected that the overall

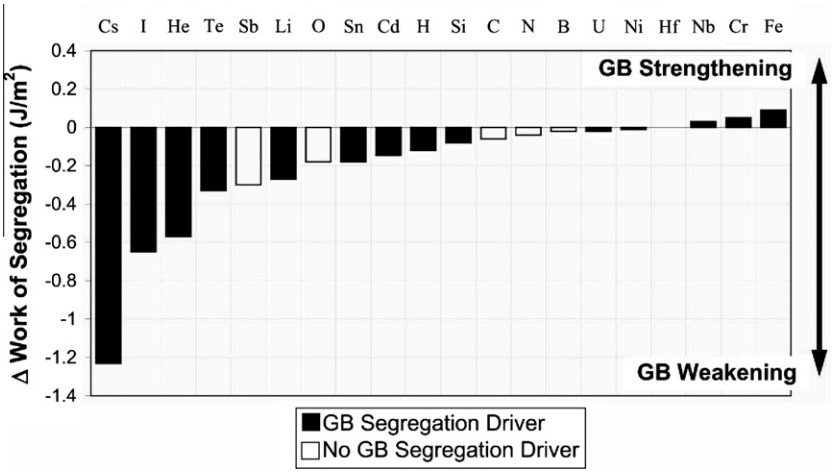

Fig. 6. Effect of impurities on the Zr grain boundary strength. Impurities are arranged from left to right in order of most weakening element (Cs) to most strengthening element (Fe).

conclusions of this study to change when entropic contributions are taken into account.

3.3. Impurities in zirconium $\sum 7$ twist grain boundary

The atomic environment of elements in a $\sum 7$ twist grain boundary is similar to that in the bulk. This leads to the same computed site preference between interstitial and substitutional sites in the grain boundary as in the bulk. Smaller elements H, He, B, C, N, and O together with Fe prefer an interstitial site within a grain boundary. A substitutional site is preferred by Li, Si, Cr, Ni, Nb, Cd, Sn, Sb, Te, I, Cs, Hf, and U, as shown in Fig. 4b for iodine. Just as in bulk zirconium, energy differences between interstitial and substitutional sites are small for elements Cr, Fe, and Ni.

Grain boundary segregation energies are given in Fig. 5. Elements showing a strong driving force for grain boundary segregation are He, Si, Cr, Fe, Ni, I, Te, and Cs. Elements that clearly prefer to stay in bulk Zr rather than in the grain boundary are C, N, and O.

Comparing grain boundary and surface segregation energies (Figs. 3 and 5), it is found that the propensity for Cr, Fe, and Nb

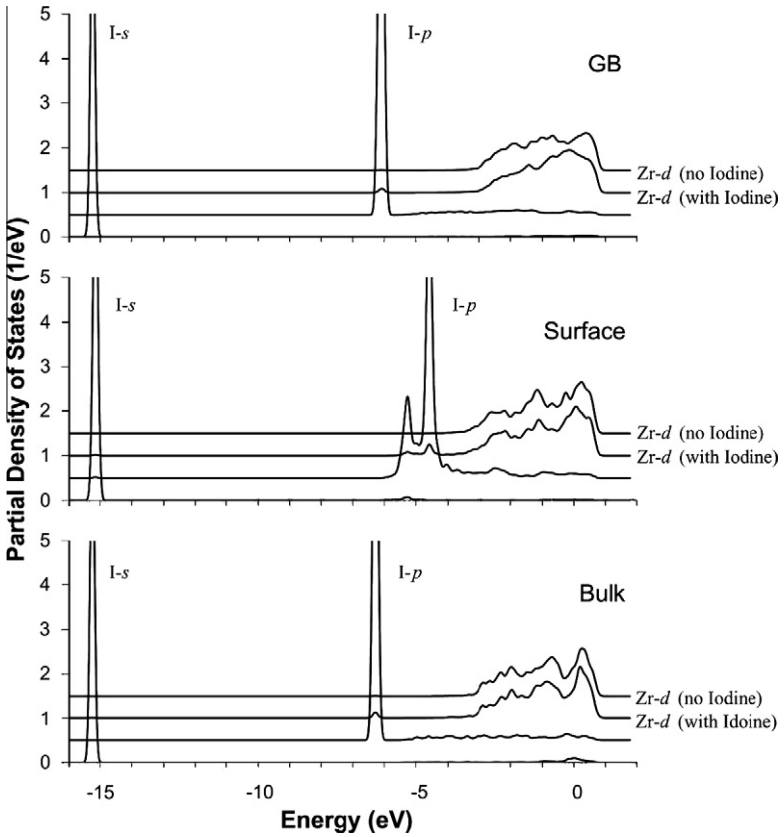

Fig. 7. Main contribution (*s* and *p*) of the PDOS for an iodine impurity, *d*-projected DOS for a neighboring Zr atom, and *d*-projected DOS for a Zr atom in the corresponding system without an impurity in the Zr bulk, at the free Zr surface, and in the Zr grain boundary.

grain boundary segregation is larger than for surface segregation. In other words, Cr, Fe, and Nb atoms tend to segregate to the grain boundary rather than to the surface. It is noted that transition metal elements Cr, Fe, and Ni have a strong tendency to migrate from the bulk to grain boundaries. In fact, grain boundary segregation energies for these elements is similar to that of I and Cs to the surface. Again, it should be pointed out that these results are for a special grain boundary and surface and may not hold for other cases.

3.4. Effects of impurities on Zr grain boundary strength

In order to assess the effects of impurities on grain boundary strength, the work of separation was calculated for the grain boundary model containing an impurity. During grain boundary decohesion, the impurity would move to an energetically more favorable position. For example, if the preferred site was substitutional in the grain boundary but as an ad-atom at the free surface, then the impurity would move to the energetically more favorable ad-atom position on fractured surface. Based on surface energy calculations, this occurred for iodine, cesium, and lithium. For all other elements, the preference for being substitutional or interstitial at the grain boundary is the same as at the free surface. The effects of impurities on the Zr grain boundary strength is displayed in Fig. 6, which shows differences in work of separation (ΔW_{sep}) for the grain boundary with and without each impurity. Cs has the largest potential for detrimental effects on a Zr $\sum$7 (0 0 0 1) grain boundary along with I, He, Te, Li, Sb, Sn, O, and H. Note that while Sb and O have a negative effect, neither have a driving force for grain boundary segregation. Fig. 6 indicates that these effects are not simply a size effect as there is no correlation between the atomic radius of an impurity and the change in work of separation. For all other elements, their effect on grain boundary strength was small. Fe had the largest strengthening effect followed by Cr and Nb. Hf has no effect on the Zr grain boundary strength, which is not surprising due to the similarity of Zr and Hf.

Electronic structure calculations were performed to further probe chemical interactions locally around an impurity atom in the Zr bulk, at the Zr free surface, and in the Zr grain boundary. Electronic structure was investigated by an angular momentum projected electronic density of states (PDOS) approach and is shown in Fig. 7 for iodine. Predicted iodine *p*-states on the free Zr surface are located at about −4 eV, closer to Zr *d*-states when compared to bulk Zr. The *p*-states are broadened at the surface and are split into a double peak. This interaction between iodine *p*-states and Zr *d*-states leads to the formation of the energetically favorable I–Zr bonding at the free Zr surface. The result is a fairly strong bond with ionic components that is highly stable for I on the Zr surface that in turn reduces the work of separation.

4. Comparing computational results to experimental fracture behavior

This section compares the results of computational studies with experimental studies assessing fission product interactions with Zircaloy cladding materials. While many studies have reported the effect of iodine interactions, two studies considered a broader field of fission products and compounds. In one study, constant extension rate tests were conducted on Zircaloy-2 at 300 °C in the presence of 35 chemical elements and several of their compounds to assess the potential for Zircaloy embrittlement [24]. Iodine produced embrittlement, with failure attributed to a SCC mechanism. Liquid metal embrittlement was reported from five metals Cd, Zn, Y, Ca, and Sr, but only when dissolved in Cs. Cs itself did not cause embrittlement. Experimentally, Cd was reported to be the most embrittling element (liquid metal mechanism), either alone or with Cs. Te was evaluated both as an element and dissolved in Cs, with only ductile fracture observed. Sb and Sn tested individually did not embrittle Zircaloy-2. Experiments with Sb, Li, or Sn dissolved in Cs were not conducted. In another study, simulated fission product elements and compounds were placed inside Zircaloy-4 tubes and either annealed at 500–1100 °C to assess chemical interactions, or pressurized and exposed to a constant temperature of 700 °C to assess creep rupture, or transient tested to 1100 °C to assess creep burst [25]. Annealing tests revealed grain boundary attack for Cd, Cs_2Te, and TeI_4, with evidence of Cd diffusion along grain boundaries. Se, Sn, Sb, Te, and I resulted in uniform attack by dissolving material at Zircaloy surfaces to form compounds. Pressurized tube studies revealed significant decreases in burst strain for Zircaloy-4 exposed to I_2, ZrI_4, TeI_4, and I_2O_5 with intergranular cracking observed on fracture surfaces and metallographic cross sections from specimens exposed to these materials as well as Te and Se. No decrement in behavior was reported for pressurized tubes containing Cs, Cd, Sn, or Sb.

Table 1
Comparison of effects of various elements on work of separation, for the Zr $\sum$7 (0 0 0 1) grain boundary, to failure modes reported in Zircaloy experimental studies.

Element	Work of Separation Zr $\sum$7 (0 0 0 1) grain boundary (J/m^2)	CERT studies at 573 K [24]	Pressurized tubes at 1073 K [25]
Cs	−1.23	Ductile	Ductile
I	−0.65	Brittle	Brittle
He	−0.57	Ductile	Ductile
Te	−0.33	Ductile	Brittle
Sb	−0.30	Ductile	Ductile
Sn	−0.18	Ductile	Ductile
Cd	−0.15	Brittle	Ductile

Table 1 compares the above computational results to experimental studies described above; mixed results are revealed. Results for iodine are consistent in both types of studies; however, results for Cs are not consistent. Cs was calculated to be the most embrittling once at a Zr $\sum$7 (0 0 0 1) grain boundary, but neither brittle intergranular nor transgranular cleavage has been reported experimentally over a wide range of conditions. This may be partially attributed to details of failure mechanisms that have not yet been explored, such as how detrimental elements interact at a crack tip to lower the strength of a boundary and kinetic transport phenomena. Mechanistic details explored with atomistic modeling studies have shown spontaneous dissociation and adsorption of iodine on a Zr Surface, accompanied by fast surface diffusion. These results implied that iodine SCC crack propagation is not likely limited by iodine diffusion [26]. Similar experimental exploration into details of Zr–I reaction kinetics has also been reported [27].

Experimental results for He not promoting brittle failure are more readily understood as there is no driving force for helium to interact with zirconium. However, helium can enter a lattice by nuclear reactions. Sources of helium may be from nuclear reactions involving trace levels of boron-10, nickel-58, alpha decay, and ternary fission. In ternary fission, a fission event produces three nuclei instead of two, with the third nucleus usually being He. He atoms produced by ternary fission have a kinetic energy of approximately 14 MeV, allowing travel of many microns in adjacent materials prior to stopping and equilibrating. While the amount of helium needed to embrittle a specific material varies on many factors, 10 atom ppm of helium has been associated with embrittlement and intergranular fracture of austenitic stainless steels above 500 °C [28]. However, He embrittlement of zirconium-based alloys has not been reported. Limited fractographic evidence from commercial PCI failures does not implicate He as an embrittling specie as characteristic void coalescence has not been observed on intergranular fracture surfaces.

5. Summary and conclusions

The strength of zirconium grain boundaries including impurity and alloying atoms was studied using first-principles DFT calculations. Interface energetics were analyzed via a concept of work of separation using a Zr $\sum 7$ (0 0 0 1) twist grain boundary model. The models utilized provide screening methods for a variety of local impurity environments to represent a range of conditions for low solute concentration in bulk, a low energy grain boundary, and a relatively higher energy material surface. Twenty different elements were investigated and ranked according to their interface energetics, including Zr grain boundary work of separation. In order of most weakening to most strengthening, the grain boundary results are: Cs, I, He, Te, Sb, Li, O, Sn, Cd, H, Si, C, N, B, U, Ni, Hf, Nb, Cr, and Fe.

These results demonstrate that the strength of the Zr $\sum 7$ (0 0 0 1) twist grain boundary is quite insensitive to most elements. This is partially due to the similar behavior of atoms in the grain boundary and at the free Zr surface. Most atoms that are energetically favorable to segregate from the bulk to the free surface are also energetically favorable to segregate to the grain boundary. Elements that prefer a substitutional site in bulk Zr also prefer a substitutional site at the surface and in the Zr $\sum 7$ (0 0 0 1) grain boundary. Exceptions are Li, I, and Cs that prefer a substitutional site in the bulk but prefer an ad-atom position at the free surface (He, which just leaves the free surface is another exception). These elements are also among those with the largest reduction in calculated grain boundary cohesion. No element in this study showed a large beneficial effect on the grain boundary strength. Comparison of modeling and experimental results reveals consistency for iodine embrittlement results.

Acknowledgements

The authors appreciate support to initiate these studies from George A. Young Jr., at Knolls Atomic Power Laboratory and programmatic support from Greg Timbol at Materials Design, Inc.

References

[1] R. Adamson, PCI details and models, in: R. Adamson (Ed.). Pellet-Cladding Interaction (PCI and PCMI), ZIRAT-11 Special Topic Report, ANT International, Sweden, October 2006, pp. 2-1–2-110.
[2] P.S. Sidky, J. Nucl. Mater. 256 (1998) 1–17.
[3] J.C. Wood, J. Nucl. Mater. 45 (1972/73) 105–122.
[4] B. Cox, J. Nucl. Mater. 172 (1990) 249–292.
[5] P. Hofmann, J. Spino, J. Nucl. Mater. 114 (1983) 50–65.
[6] J.R. Wu, A.J. Freeman, G.B. Olson, Science 265 (1994) 376.
[7] W.T. Geng, A.J. Freeman, R. Wu, C.B. Geller, J.E. Raynolds, Phys. Rev. B 60 (1999) 7149.
[8] G.A. Young Jr., R. Najafabadi, W. Strohmayer, D.G. Baldrey, W.L. Hamm, J. Harris, J. Sticht, E. Wimmer, An atomistic modeling study of alloying element, impurity element, and transmutation products on the cohesion of a nickel $\sum 5$ {0 0 1} twist grain boundary, in: 11th International Conference on Environmental Degradation of Materials in Nuclear Power Systems – Water Reactors, Stevenson, Washington, August 10–14 2003.
[9] W. Zhang, J.R. Smith, X.-G. Wang, A.G. Evans, Phys. Rev. B 67 (2003) 245414.
[10] M. Christensen, G. Wahnstrom, Acta Mater. 52 (2004) 2199.
[11] M. Christensen, G. Wahnstrom, Int. J. Refract. Metal. Hard Mater. 24 (2006) 80.
[12] (a) Hohenberg, W. Kohn, Phys. Rev. 136 (1964) B864;
(b) W. Kohn, L.J. Sham, Phys. Rev. 140 (1965) Al 133.
[13] J.P. Perdew, K. Burke, M. Ernzerhof, Phys. Rev. Lett. 77 (1996) 3865.
[14] P.E. Blochl, Phys. Rev. B 50 (1994) 17953.
[15] G. Kresse, J. Hafner, Phys. Rev. B 47 (1993) 558.
[16] G. Kresse, J. Furthmuller, Phys. Rev. B 54 (1996) 11169.
[17] G. Kresse, J. Furthmuller, Comput. Mater. Sci. 6 (1996) 15.
[18] G. Kresse, D. Joubert, Phys. Rev. B 59 (1999) J758.
[19] MedeA 2.3, Materials Design, Inc., Angel Fire, NM, 2007.
[20] R.B. Russel, J. Appl. Phys. 24 (1953) 232.
[21] P. Blochl, O. Jepsen, O.K. Andersen, Phys. Rev. B 49 (1994) 16223.
[22] S.K. Kwon, Z. Nabi, K. Kadas, L. Vitos, J. Kollar, B. Johansson, R. Ahuja, Phys. Rev. B 72 (2005) 235423.
[23] P. Villars (Editor-in-chief), File Binaries Edition, Version 1.0, ASM International, 2002.
[24] W.T. Grubb, M.H. Morgan III, Am. Soc. Test. Mater. (1979) 145–154.
[25] P. Hofmann, J. Spino, J. Nucl. Mater. 102 (1981) 117–134.
[26] M. Christensen, T.M. Angeliu, J.D. Ballard, J. Vollmer, R. Najafabadi, E. Wimmer, in: Proceedings of TOP FUEL 2009, French Nuclear Energy Society, Paper 2165, 2009.
[27] M. Balooch, D.R. Olander, J. Electrochem. Soc. 130 (1983) 151–157.
[28] W. Kesternich, J. Nucl. Mater. 127 (1985) 153–160.